POSITION PAPER

Guidelines for the assessment of bone density and microarchitecture in vivo using high-resolution peripheral quantitative computed tomography

D.E. Whittier[1,2] · S.K. Boyd[1,2] · A.J. Burghardt[3] · J. Paccou[4] · A. Ghasem-Zadeh[5] · R. Chapurlat[6,7] · K. Engelke[8,9] · M.L. Bouxsein[10,11]

Abstract

Introduction The application of high-resolution peripheral quantitative computed tomography (HR-pQCT) to assess bone microarchitecture has grown rapidly since its introduction in 2005. As the use of HR-pQCT for clinical research continues to grow, there is an urgent need to form a consensus on imaging and analysis methodologies so that studies can be appropriately compared. In addition, with the recent introduction of the second-generation HrpQCT, which differs from the first-generation HR-pQCT in scan region, resolution, and morphological measurement techniques, there is a need for guidelines on appropriate reporting of results and considerations as the field adopts newer systems.

Methods A joint working group between the International Osteoporosis Foundation, American Society of Bone and Mineral Research, and European Calcified Tissue Society convened in person and by teleconference over several years to produce the guidelines and recommendations presented in this document.

Results An overview and discussion is provided for (1) standardized protocol for imaging distal radius and tibia sites using HR-pQCT, with the importance of quality control and operator training discussed; (2) standardized terminology and recommendations on reporting results; (3) factors influencing accuracy and precision error, with considerations for longitudinal and multi-center study designs; and finally (4) comparison between scanner generations and other high-resolution CT systems.

Conclusion This article addresses the need for standardization of HR-pQCT imaging techniques and terminology, provides guidance on interpretation and reporting of results, and discusses unresolved issues in the field.

Keywords Bone microarchitecture · Guidelines · High-resolution peripheral quantitative computed tomography · Imaging protocol

Introduction

High-resolution peripheral quantitative computed tomography (HR-pQCT) is a non-invasive, low-radiation approach for assessing compartment-specific volumetric bone mineral density and bone microarchitecture in the peripheral skeleton, most commonly the distal radius and tibia. Until the introduction of the first HR-pQCT device in 2005 [1], assessment of human bone

✉ M.L. Bouxsein
mbouxsei@bidmc.harvard.edu

1 McCaig Institute for Bone and Joint Health, Cumming School of Medicine, University of Calgary, Calgary, AB, Canada

2 Department of Radiology, Cumming School of Medicine, University of Calgary, Calgary, AB, Canada

3 Department of Radiology and Biomedical Imaging, University of California, San Francisco, CA, USA

4 Department of Rheumatology, MABlab UR 4490, CHU Lille, Univ. Lille, 59000 Lille, France

5 Departments of Endocrinology and Medicine, Austin Health, The University of Melbourne, Melbourne, Australia

6 INSERM UMR 1033, Université de Lyon, Lyon, France

7 Hôpital Edouard Herriot, Hospice Civils de Lyon, Lyon, France

8 Department of Medicine 3, FAU University Erlangen-Nürnberg and Universitätsklinikum Erlangen, Erlangen, Germany

9 Bioclinica, Inc., Hamburg, Germany

10 Center for Advanced Orthopedic Studies, Beth Israel Deaconess Medical Center, Boston, MA, USA

11 Harvard Medical School, Boston, MA, USA

microarchitecture was largely limited to histomorphometric or micro-CT analysis of iliac crest biopsies [2, 3] or technically challenging, limited resolution micro-magnetic resonance imaging. The ability to investigate bone microarchitecture in vivo has provided novel insights into differences due to age, sex, and ethnicity [4–13]; changes due to disease [14–17]; response to nutritional and pharmacologic treatments [18–22]; the impact of physical activity [23–26]; and deficits associated with increased fracture risk [27]. The use of HR-pQCT for clinical research studies has grown rapidly in the past decade, and as its application continues to expand, there is a need to establish recommendations for best practices and to discuss unresolved issues related to its use in clinical studies. Furthermore, with the recent introduction of a second-generation HR-pQCT device with improved resolution and longer scan region, it is important to highlight the differences and comparability between scanner generations, future HR-pQCT devices, and alternative systems, such as cone-beam CT.

Thus, the objective of this manuscript is to provide guidance on the technical aspects of HR-pQCT for use in the clinical setting, including best practices for acquisition and analysis of scans, as well as provide guidance on the presentation and interpretation of results. The work presented here is a product of a joint IOF-ASBMR-ECTS working group, which met in person and by teleconference over several years to produce this document. The final document was endorsed by the IOF, ASBMR, and ECTS.

Overview of HR-pQCT techniques

The following sections describe the steps involved in the conventional evaluation of bone mineral density and microarchitecture in vivo using HR-pQCT. Each section provides the best practices and considerations when conducting clinical studies. In most cases, the first-generation HR-pQCT (XtremeCT, Scanco Medical AG, Brütiselen, Switzerland) is used as a standard for outlining each step, as it is widely used today. However, these practices are intended to be applicable broadly to other HR-pQCT scanners, namely the second-generation HR-pQCT (XtremeCT II, Scanco Medical AG, Brütiselen, Switzerland), as well as future devices that may be developed by other manufacturers. The basic steps include image acquisition, image processing, image analysis, and reporting of results.

Imaging principles and radiation dose

HR-pQCT provides a method to non-invasively and three-dimensionally evaluate bone mineral density and microarchitecture at high resolutions. The benefit of HR-pQCT over comparable micro-CT systems is the ability to obtain images of human extremities in vivo due to the relatively larger gantry size, at the compromise of somewhat reduced resolution.

The basic imaging principles are based on the interaction of ionizing radiation (i.e., X-rays) with matter. As an X-ray beam passes through matter, it is attenuated in relation to the density of the matter, with denser materials such as bone, resulting in greater attenuation than low-density materials, such as soft tissue. In computed tomography, X-ray attenuation data is acquired at multiple projections around the specimen, which allows for a 3D image to be reconstructed [28]. The effective radiation dose from a standard HR-pQCT scan at the distal radius or tibia is 3–5 μSv depending on the scanner generation [29]. In comparison with other common medical imaging techniques, this is considered a low radiation dose procedure. For example, a hip scan using dual-energy X-ray absorptiometry (DXA), commonly used for monitoring osteoporosis, has an effective dose of approximately 9 μSv, a standard chest X-ray has an effective dose of approximately 100 μSv, and a hip CT scan has an approximate effective dose of 286–506 μSv [30, 31].

Image acquisition

Positioning and selection of scan region

Properly positioning the patient's limb in the scanner and identifying the appropriate scan region are fundamental to all imaging protocols. The limb should be immobilized to minimize motion and properly positioned by using a padded, anatomically formed carbon fiber cast provided by the manufacturer. If not scanning bi-laterally, the technician should scan the non-dominant limb, unless prior fracture, surgery, or metal is present, in which case the contralateral side should be scanned.

Once the limb is placed into the gantry of the scanner, a 2D scout view is obtained to select the region of interest for the 3D measurement (this process takes approximately 2–4 min per limb). There are then two approaches used to define the region where the scan is acquired: (1) fixed offset distance and (2) relative offset distance, also called the %-of-length offset. For the fixed offset method, the operator places a reference line at the inflection point on the endplate of the distal radius or tibial plafond, and the scan region begins 9.5 mm and 22.5 mm proximal to the reference line for the radius and tibia, respectively (Fig. 1). The scan region then extends proximally from this point by 9.02 mm (110 slices) for first-generation scanners and 10.20 mm (168 slices) for second-generation scanners [1, 32]. This approach has been implemented in early studies using the second-generation HR-pQCT [32, 33]; however, due to the increased scan region, an additional 1.0 mm is acquired proximally, a predominantly cortical region. As a result, the manufacturer recommendation for the second-generation HR-pQCT is to use a fixed offset of 9.0 mm and 22.0 mm proximal to the reference line for the radius and tibia, respectively [29]. This difference positions the scan region so that it aligns with the center of the first-generation scan region, extending an additional 0.5 mm in both the proximal and distal region.

Fig. 1 Scout view from a first-generation HR-pQCT showing reference line placement for the fixed offset distance (left) and relative offset distance (right) methods for the radius and tibia [36]. The edge of the radiocarpal joint surface of the distal radius and tibial plafond are marked in red. Scan regions represented here are approximate and illustrate a scenario where the fixed and relative offsets are aligned
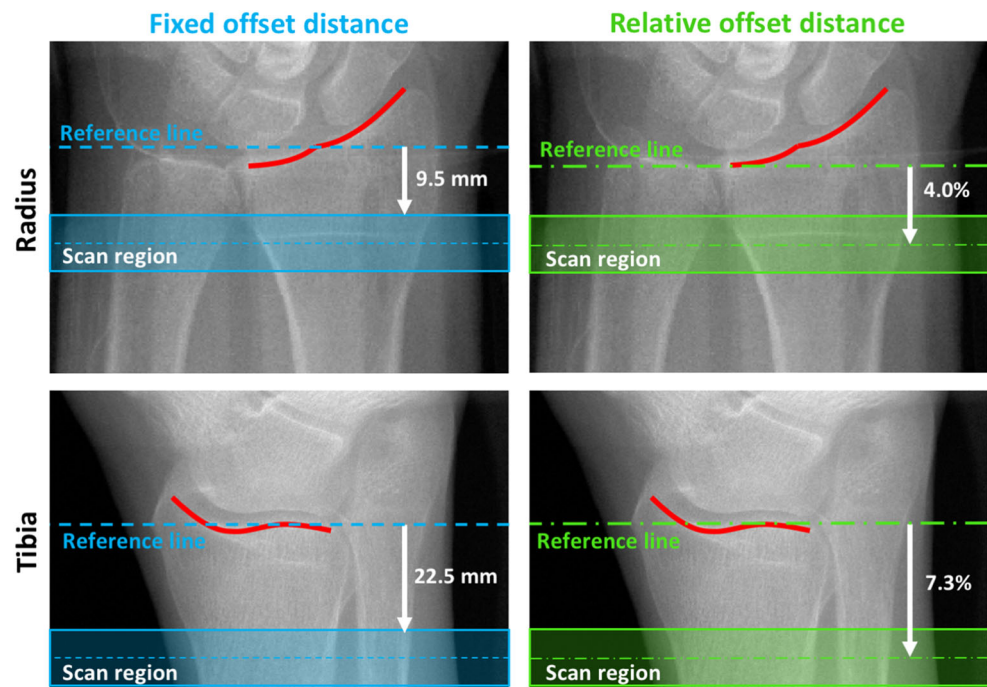
In the %-of-length approach, the operator measures the limb length and then selects a certain percent of the limb length, depending on the specific protocol, as the center point for the scan region. In this approach, the reference line placement is identical as above for the tibia, but for the radius, the reference line is placed at the proximal margin of the radial head (Fig. 1) [34, 35].

The limitation of a %-of-length measure is that it requires an accurate external physical limb length measurement prior to scanning, and it assumes that bone regions (epiphysis, metaphysis, and diaphysis) are proportional to limb length. The ulnar length is recommended as a surrogate for radial length because it is more reliable to identify the distal and proximal ends of the ulna. The ulnar length should be taken as the Euclidean distance between a horizontal surface on which the elbow is rested and the styloid process at the wrist. The tibial length should be taken as the Euclidean distance between the tibial plateau at the knee and the medial tibial malleolus at the ankle [36]. For a detailed description of measurement methods, we recommend the guidelines provided by Bonaretti and colleagues [36]. If using a %-of-length offset, for adults, we recommend the scan position be centered at 4.0% offset from the proximal margin of the radiocarpal joint surface of the distal radius, and 7.3% offset from the tibial plafond (Fig. 1). These relative offsets align, on average, with the standard fixed-length offset of the first-generation scanner. Centering the scan offset in this way yields equivalent variability in distal and proximal directions, minimizing bias introduced by differences in the relative length of the measured limb [37]. In longitudinal studies in adults, limb length should be measured at baseline, and the same length measurement used at follow-up visits in lieu of repeating the limb length measurement at each follow-up time point.

To date, most HR-pQCT studies in adults have employed the fixed offset distance approach, though this method is likely to confound the interpretation of results for studies that compare groups of differing heights (and therefore limb length), such as comparisons by sex and race/ethnicity, and even age, due to secular trends in limb length [37–40]. This is because a fixed distance offset from an anatomic reference results in measurements that are acquired at a relatively "too" distal location in individuals with long limbs and relatively "too" proximal position in individuals with short limbs. These differences cannot necessarily be made equivalent by statistical adjustment for height or limb length [37]. However, while the bone microarchitecture in the metaphyseal region is highly variable as a function of limb length [38], the difference in scan location between a relative (%-of-length) and a fixed offset approach is generally small. Nevertheless, an individual with a stature that is different from the population mean will have some measurement bias exceeding typical motion-induced errors due to positioning from a fixed offset [37, 41].

Another form of measurement error that arises from reference line placement is operator-driven variability. Bonaretti and colleagues reported that intra-operator variability in scan positioning corresponds to up to 4% of the total scan length, while inter-operator positioning variability is up to 7.5% of the total scan length [42]. This translates to significant measurement precision error, often exceeding the precision error attributable to subject motion. Standardized training for scan positioning, described by Bonaretti and colleagues, can reduce operator positioning error by approximately half [42].

In addition to the conventional scan region, it is possible to acquire scans more proximal to the standard position in order to investigate predominantly cortical bone, either as a proximal subset of slices extracted from a standard distal scan [43], an additional contiguous scan [44], or an independent scan proximal to the standard position [26, 45, 46]. Accordingly, there is some evidence that more proximal locations along the radius and tibia provide greater sensitivity to cortical bone changes. The second-generation HR-pQCT allows greater access to proximal scan positions at the forearm and tibia, and it is now possible to develop diaphyseal scan protocol centered at 30% of the ulnar/tibial length using the standard leg and forearm casts, and up to 66% of ulnar/tibial length using custom casts. Acquisition of scans at these regions allows for additional measurement of cortical bone, muscle, and fat, analogous to lower resolution pQCT [47, 48]; however, development of standardized scan acquisition and analysis protocols is ongoing.

In summary, it is recommended that research centers transition to a standardized protocol in future study designs, using the %-of-length offset scan region described above. However, given the historical use of a fixed offset scan region, there exist valuable cross-sectional and longitudinal datasets worldwide based upon this scan protocol. Consequently, the use of the fixed offset is an acceptable alternative, should studies need to compare results to historical databases. Due to differences across research centers, it is important to report in all publications how the scan region was selected, including choice of reference line placement, type of offset (fixed vs. relative), distance of offset, and total scan length.

Scan acquisition and motion artifacts

Scan acquisition varies depending on the in vivo measurement protocol, which is scanner and study specific. The standard protocol and scanner specifications for the commonly used HR-pQCT scanners, XtremeCT and XtremeCT II, are summarized in Table 1.

Scanned images should be inspected visually for motion artifacts, especially at the distal radius due to higher prevalence of motion at this location. Subject motion during image acquisition can lead to degraded image quality and introduce error, particularly for trabecular and cortical microarchitecture [41, 49, 50]. To determine what degree of motion is acceptable, several grading scales have been developed, where the most commonly used is a 5-level motion grading scale (best score is 1, worst score is 5) that aims to differentiate motion on the severity of artifacts, summarized in Fig. 2 [41]. However, even with a standardized scoring system, motion scoring remains subjective, and operator agreement has shown to remain only moderate, even with intensive training [49–51]. Automatic techniques analyzing CT projections have been suggested to provide a standardized approach [50]; however, these procedures have not yet been integrated into HR-pQCT protocols. Until automated techniques are integrated, the 5-level grading scale is recommended, with scoring done consistently by the same operator where possible. At the time of scanning, if motion artifacts with a score of three or more are observed, then it is recommended the scan be repeated.
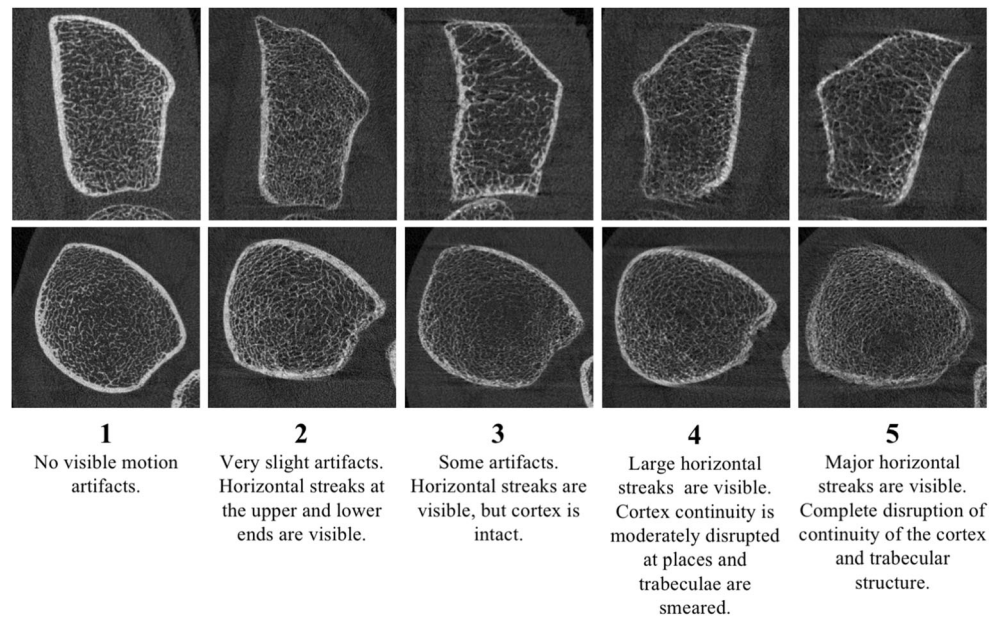
In general, density-based measures are less sensitive to motion artifacts than structure-based measures. It is acceptable to include all outcome variables from scans with a motion score of three or less, as the precision error is not substantially compromised for density (< 1% error), microarchitecture (< 5% error), and biomechanical parameters, such as estimated failure load (< 4% error) [50]. Scans with a motion score of four may be acceptable for density-based measurements, but should not be used for

Table 1 Technical parameters of first-generation (XtremeCT) and second-generation (XtremeCT II) HR-pQCT standard in vivo scan protocol. Technical specifications adapted from Manske et al. [32]

	First-generation HR-pQCT (XtremeCT)	Second-generation HR-pQCT (XtremeCT II)
Technical specifications		
Energy (kVp)	59.4	68.0
Current (μA)	900	1470
Integration time (ms)	100	43
Field of view (cm)	12.6	14.0
Scan time (min)	2.8	2.0
Stack length (mm)	9.02	10.2
Isotropic voxel size (μm)	82.0	60.7
Spatial resolution (μm)	134.6–154.4	92.5–112.6
Effective patient dose (μSv)	3–5	5
Standard image processing specifications		
Image filtering	Laplace-Hamming filter: ε 0.5, cut-off 0.4	Gaussian filter: σ 0.8, support 1.0
Bone volume segmentation threshold	Global threshold: 400 permille (‰)	Trabecular: 320 mg HA/cm^3, Cortical: 450 mg HA/cm^3
Morphological analysis	Direct and derived measurements	Direct measurements

Fig. 2 Motion grading guideline as recommended by the manufacturer and presented by Sode et al. [41], with visual examples provided here for second-generation HR-pQCT radius (top row) and tibia (bottom row) scans

1 No visible motion artifacts.

2 Very slight artifacts. Horizontal streaks at the upper and lower ends are visible.

3 Some artifacts. Horizontal streaks are visible, but cortex is intact.

4 Large horizontal streaks are visible. Cortex continuity is moderately disrupted at places and trabeculae are smeared.

5 Major horizontal streaks are visible. Complete disruption of continuity of the cortex and trabecular structure.

trabecular and cortical microarchitecture or biomechanical assessment. Scans with a motion artifact score of 5 should not be used.
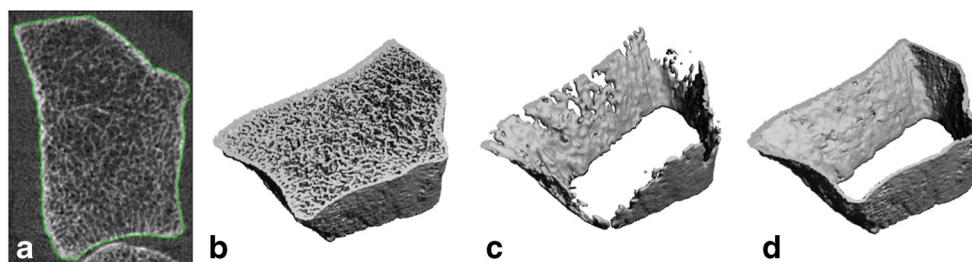
Image processing

Segmentation of the cortical and trabecular bone compartments is necessary for density and structural analysis. Over the past decades, automated and semi-automated methods have been developed to improve accurate and repeatable extraction of the cortical and trabecular compartments.

Standard vs. extended cortical analysis

In the first-generation HR-pQCT standard analysis, the operator guides a semi-automated slice-by-slice contouring process to identify the periosteal boundary of the bone, thereby extracting the bone region from surrounding soft tissue (Fig. 3a). The bone region is extracted using a Laplace-Hamming filter and global threshold cut-off of 400 permille (‰) to generate the segmented bone volume be used for proceeding morphological analysis (Fig. 3b). Delineation of the cortical and trabecular compartments is done automatically using a filter and threshold-based algorithm, where the original greyscale bone region is smoothed using a high-Gaussian weighted filter, then a cut-off of 160 permille (‰) is used to identify voxels that belong to cortical bone [52]. However, this method is insufficient for extraction of the cortex when it is thin and/or highly porous (Fig. 3c) [53, 54] or when the trabecular structure is rich and well connected to the cortex. Thus, an alternate algorithm, the so-called "extended cortical analysis" which uses a dual-threshold segmentation technique, has been incorporated to provide a more robust extraction of the cortical and trabecular compartments [55, 56]. It involves a two-step algorithm to automatically identify the periosteal and then the endocortical surface. In the first step, a connectivity filter is applied to the previously generated segmented bone volume to create a mask of the whole bone region. In the second step, a dilation-erosion operation is applied to the background (i.e., marrow cavity) of the original segmented bone volume to remove trabeculae, thus leaving a mask of the cortical compartment (Fig. 3d) [55]. Once the compartments are defined, the

Fig. 3 Example of distal radius scan from a first-generation HR-pQCT and outputs from image processing protocol, where **a** is the greyscale slice-wise view with the periosteal contour (green) identified, **b** segmented whole bone volume, **c** cortical bone region extracted using the standard analysis protocol, and **d** cortical bone region extracted using the dual-threshold technique

extended cortical analysis allows for the assessment of cortical porosity and cortical tissue mineral density, as well as a direct measure of cortical thickness, described in detail in the later sections. With the deployment of the second-generation HR-pQCT scanner, the dual-threshold technique is the default segmentation method, and the image filtration and segmentation thresholds have been adjusted to account for the increased resolution, summarized in Table 1.

Manual correction

Although the dual-threshold technique improves the segmentation of the cortical and trabecular compartments, errors can persist. It is imperative that operators check the periosteal and endocortical contours visually for errors and apply manual corrections as necessary. Omitting corrections of the automatically generated contours leads to greater accuracy errors arising in very low- or high-density bone, resulting in a systematic bias with certain parameters, such as cortical density and thickness [57]. This has the potential to skew the results of studies that investigate osteoporotic or highly active populations; therefore, we advise that contours be checked and manually corrected [57].

Drawbacks to manual corrections include the increased time spent visually inspecting images and the potential for increased precision error that arises when manual corrections are applied [58, 59]. In particular, the endocortical contour can be highly subjective in low-density bone, and human interpretation by one or more operators introduces precision error. Nevertheless, inter-operator variability introduces less error than the accuracy error resulting from uncorrected contours [59], and short-term precision between using corrected versus uncorrected contours is comparable [58]. If manual corrections are applied, it is essential the operator has a suitable level of training to minimize precision error [57].

Image analysis

The defined cortical and trabecular compartments are the basis for measuring density and microarchitecture properties. Tables 2 and 3 provide a summary of common parameters, units, and methods of measurement from HR-pQCT modalities as have been previously described in the literature [1, 32].

Trabecular microarchitecture

Trabecular microarchitecture is assessed from the segmented image; however, the spatial resolution of the first-generation HR-pQCT limits the ability to measure trabecular thickness, and as a result, some of the trabecular morphology measures are derived using 2D stereologic methods rather than directly measured. Specifically, trabecular bone volume fraction (Tb.BV/TV) is computed as the ratio of the trabecular bone mineral density (Tb.BMD) and 1200 mg HA/cm^3, which is

assumed to be the density of fully mineralized bone (Table 3). Alternatively, trabecular number (Tb.N) is directly measured using a ridge extraction technique [52]. Trabecular separation (Tb.Sp) and trabecular thickness (Tb.Th) are then derived from these two parameters assuming a plate-like morphology, as described in Table 3 [60].

In contrast, the second-generation HR-pQCT has sufficient spatial resolution to "directly" measure Tb.BV/TV, Tb.Th, and Tb.Sp. Accordingly, Tb.BV/TV is defined as the ratio of voxels in the mineralized bone phase to the total number of voxels in the trabecular compartment. Tb.Sp and Tb.Th are measured using the distance transformation method, where 3D distances are estimated by fitting maximal spheres inside the structure (or void space in the case of Tb.Sp) and taking the average sphere diameter as the mean thickness [61].

In addition to common morphometric indices, additional parameters have been developed to estimate the level of anisotropy in trabecular microarchitecture from HR-pQCT images. These non-metric indices include the structure model index (SMI) [60], connectivity density (Conn.D) [62], and mean intercept length (MIL) [63], outlined in Table 3. Another non-standard analysis includes individual trabecular bone segmentation (ITS)–based morphological analysis [64]. This approach performs a complete volumetric decomposition of individual trabecular plates and rods to characterize bone morphology and orientation of trabecular bone. These non-standard analyses are susceptible to resolution effects and demand cautious interpretation.

Cortical microarchitecture

Primary cortical microarchitecture parameters include the cortical thickness (Ct.Th) and cortical porosity (Ct.Po). The standard analysis for first-generation HR-pQCT derives Ct.Th from the mean cortical volume divided by the periosteal surface area. However, in the extended cortical analysis, the cortical thickness is directly measured using distance transformation methods once the cortical compartment has been extracted using the dual-threshold segmentation technique. Measurement of Ct.Po is limited by the spatial resolution of the HR-pQCT images, as Haversian canals can range in size from 30 to 350 μm. However, it is estimated that pores smaller than 90 μm contribute to only 5–8% of the total pore volume [65]. Measurement of Ct.Po is improved with the second-generation of HR-pQCT due to increased resolution [33].

Two methods currently exist to assess Ct.Po: (1) the threshold-based approach [55, 56] implemented in the XtremeCT analysis software provided by Scanco and (2) the density-based approach implemented in the StrAx1.0 software [43]. The threshold-based approach is a fully automated segmentation contouring approach integrated with extended

Table 2 Definition, units, and measurement of methods of common whole bone and cortical microarchitecture parameters obtained from available HR-pQCT systems. Italicized parameters are the minimum set to be reported when describing cortical bone morphology

Parameter	Abbreviation and standard units	Description	Measurement method	
			XtremeCT	XtremeCT II
Densities and areas				
Total bone mineral density	**Tt.BMD (mg HA/cm^3)**	Average mineral density within the periosteal surface	Calculated directly from the greyscale image data	
Cortical bone mineral density	**Ct.BMD (mg HA/cm^3)**	Average mineral density within the cortical compartment	Calculated directly from the greyscale image data	
Cortical tissue mineral density	Ct.TMD (mg HA/cm^3)	Average mineral density of the segmented cortical bone	Calculated directly from the greyscale image data, after pores have been masked from the region of interest.	
Total area	Tt.Ar (mm^2)	Measure of total cross-sectional area within the periosteal surface	Mean cross-sectional area of cortical compartment in all image slices	
Cortical area	Ct.Ar (mm^2)	Measure of the total cross-sectional area within the cortical bone compartment	Mean cross-sectional area of region within periosteal surface in all image slices	
Cortical bone microarchitecture				
Cortical thickness	**Ct.Th^d| Ct.Th (mm)**	Average thickness of the cortical compartment	Volume of the cortical compartment divided by the periosteal surface[†]	Mean spacing of the periosteal and endocortical surfaces, measured using the distance transformation method[*]
Cortical perimeter	Ct.Pm (mm)	Length of periosteal perimeter	Mean of periosteal perimeter in all image slices	
Cortical porosity	**Ct.Po^d| Ct.Po (%)**	Ratio of pore volume relative to the total volume of the cortical compartment, reported in percentage	Threshold-based approach: Ratio of volume of pores relative to the total volume in the cortical compartment[*] Density-based approach: The ratio of voxel-by-voxel void space to fully mineralized bone (1200 mg HA/cm^3) in compact cortical compartment[‡]	
Cortical pore volume	Ct.Po.V (mm^3)	Total volume of cortical pores	Summation of pore voxels in the intra-cortical region[*]	
Cortical pore diameter	Ct.Po.Dm (mm)	Average 3D diameter of the pore volumes	Mean spacing of the segmented cortical pores using the distance transform method[*]	

[d] Superscript should be used if reporting results using the derived measurement method

[*] Description of direct 3D morphological method of measurement

[†] Description of derived (indirect) morphological method of measurement

[‡] StrAx is a derived method with analysis bone compartments defined differently than the extended cortical analysis [55, 56] and is not integrated into the Scanco workflow

Ideally the minimum set of parameters reported are bolded

cortical analysis method. Briefly, intra-cortical porosity (Ct.Po) is calculated as the ratio of the total pore volume within the cortical compartment to the sum of the cortical volume [56]. This method has the advantage of segmenting the individual pores from the scan, which allows for structural information to be measured, including mean cortical pore diameter (Ct.Po.Dm); however, it is limited to capturing only pores within the limits of resolution and pores that do not intersect the periosteal or endocortical surfaces.

Alternatively, the density-based approach segments bone into a compact-appearing cortex, transitional zone, and trabecular compartment, described in detail elsewhere by Zebaze and colleagues [43]. In brief, Ct.Po is quantified in each of these regions by assuming that fully mineralized bone has a density between 1000 and 1200 mg HA/cm^3. Voxels with a density lower than 1000 mg HA/cm^3 indicate that some ratio of the voxel, proportional to its density, is composed of void space (i.e., pores). Porosity is quantified by estimating the ratio of void space present in each voxel and taking the mean across all voxels in the compartment of interest [43]. The density-based method of assessing Ct.Po aims to capture pores with diameters below the spatial resolution of the scanner; however, it relies on the assumption of a fixed bone tissue mineral density and is susceptible to image noise and beam hardening.

Table 3 Definition, units, and measurement of methods of common trabecular microarchitecture parameters obtained from available HR-pQCT systems. Italicized parameters are the minimum set to be reported when describing trabecular bone morphology

Parameter	Abbreviation and standard units	Description	Measurement method	
			XtremeCT	XtremeCT II
Density and area				
Trabecular bone mineral density	**Tb.BMD (mg HA/cm³)**	Average mineral density within the trabecular compartment	Calculated directly from the greyscale image data	
Trabecular area	Tb.Ar (mm²)	Cross-sectional area of the trabecular compartment	Mean cross-sectional area of trabecular compartment in all image slices	
Trabecular bone microarchitecture				
Trabecular bone volume fraction	**Tb.BV/TV[d]** | **Tb.BV/T-V (%)**	Ratio of segmented bone volume to total volume of the trabecular compartment, reported as a percentage.	(Tb.BMD/1200 mg HA/cm³) × 100[†]	Ratio of voxels in the mineralized bone phase to the total number of voxels in the trabecular compartment[*]
Trabecular number	**Tb.N (1/mm)**	Average number of trabeculae per unit length	Mean inverse of the spacing between mid-axis (ridges) of the trabeculae. Ridges are identified using ridge extraction technique[*]	
Trabecular separation	**Tb.Sp[d]** | **Tb.Sp (mm)**	Average distance between trabeculae	(1 − BV/TV)/Tb.N[†]	Mean separation between trabeculae measured using the distance transformation method applied to the background (void space) of the structure[*]
Trabecular thickness	**Tb.Th[d]** | **Tb.Th (mm)**	Average thickness of trabeculae	Ratio of BV/TV to Tb.N[†]	Mean spacing of the segmented trabecular structure, measured using the distance transformation method[*]
Inhomogeneity of trabecular network	Tb.1/N.SD (mm)	Measure of inhomogeneity of trabecular separation	The standard deviation of the spacing between mid-axis (ridges) of the trabeculae[*]	
Structural model index	SMI (unitless)	Quantification of structural appearance of trabeculae	Calculated from the derivative of the trabecular bone surface area. SMI of 0 indicates plate-like structure, 3 indicates rod-like structure, and 4 indicates sphere-like structure [60].	
Connectivity density	Conn.D (1/mm³)	Measure of the connectivity of the trabeculae	Calculated using the Conn-Euler method [62]	
Degree of anisotropy	DA (unitless)	Measure of the anisotropy of the trabecular structure.	Estimated as the longest divided by the shortest principal directions of the mean intercept length ellipsoid. A DA of 1 is isotropic.	

[d] Superscript should be used if reporting results using the derived measurement method

[*] Description of direct 3D morphological method of measurement

[†] Description of derived (indirect) morphological method of measurement

Ideally the minimum set of parameters reported are bolded

A comparison of methods for in vivo assessment of Ct.Po revealed that both approaches are well correlated with gold standard porosity measurements from synchrotron radiation micro-computed tomography (SRμCT); however, each method has inherent systematic errors. In compact-appearing cortical bone specimens, the threshold-based approach underestimates Ct.Po by 3 to 11% as it does not capture smaller pores, whereas the density-based approach overestimates Ct.Po by 6 to 21% due to misclassifying image noise and artifacts as void space [65]. The threshold-based approach has improved accuracy in Ct.Po measurements with the second-generation HR-pQCT as this approach is resolution-dependent, whereas the density-based approach would not be impacted as it is not resolution-dependent. Both methods are widely adopted measures of Ct.Po, but due to methodologic differences, they cannot be directly compared and study methodologies should clearly state which method is used.

Finite element analysis

Morphometric parameters are numerous and provide valuable insight describing the structure of a bone, but the interpretation of these data can be complex. Finite element (FE) analysis is a computer modeling technique that, when coupled with HR-pQCT, provides a non-invasive approach to intrinsically account for the complex bone structure and estimate bone strength [66]. The fundamental requirements for an FE model are selecting the bone geometry, assigning material properties, and defining boundary conditions to simulate loading

conditions, typically determined through validation studies using experimental loading tests of cadaveric bones [67–69]. The application of FE procedures to HR-pQCT images has been explored in depth and is often referred to as micro-FE (μFE). Most HR-pQCT-based μFE models to date have defined constitutive properties that are linear, with uniform elastic material properties. However, non-linear models and density-based elastic material properties have also been implemented [67, 70–72]. Here, we outline key considerations and recommendations when choosing a μFE procedure, with a specific focus on linear, homogeneous models for standard HR-pQCT scan regions.

Model generation and boundary conditions

Geometry is determined from the segmented HR-pQCT image by converting it into an FE mesh, most commonly using a voxel-by-voxel conversion where each voxel is converted into a cubic hexahedral finite element [73]. First-generation HR-pQCT images typically result in FE models with 1–9 million elements [66] and second-generation in the range of 2–24 million elements, depending on the scan site and bone volume, resulting in a direct representation of the bone microarchitecture (Fig. 4).

Boundary conditions are selected to simulate a loading condition. Standard HR-pQCT scans are best suited for simulating a compression test along the z-axis (longitudinal axis), defined perpendicular to scan cross-section. One end is assigned a fixed constraint in the z-direction and a fixed displacement is applied to the opposite end resulting in 1% apparent strain. If the fixed constraint surface includes conditions that prevent lateral expansion during compression, the test is referred to as axial compression; otherwise, it is termed a uniaxial compression. The results of a compression test will differ slightly depending on whether axial or uniaxial boundary conditions are applied, but they are strongly linearly associated ($r^2 > 0.99$), and methods have been developed to allow harmonization by applying a linear correction factor [74].

Material properties must also be defined for the model, including Poisson's ratio and the elastic modulus (also called the tissue modulus or Young's modulus). A Poisson's ratio of 0.3 is conventionally used for all μFE models. However, selection of the elastic modulus requires closer consideration as it ultimately defines the stiffness of the material under tension or compression. The most common approach is to assign a uniform elastic modulus, previously determined through direct comparison to experimental loading tests, to all bone tissue in the model. A summary of common elastic modulus values (and their respective boundary conditions) for first- and second-generation HR-pQCT scanners are summarized in Table 4. The modulus utilized for a given scanner generation will not yield the same results if applied to another generation, as the elastic modulus is dependent on both the mesh resolution and segmentation

protocol, which impact the bone structure extracted from the image. Hence, for second-generation HR-pQCT, an elastic modulus of 8748 MPa has been back-calculated from the modulus validated for the first-generation HR-pQCT [74], and 10,000 MPa has been determined from direct comparison to experimental loading tests [68].

FE outcomes

Table 5 provides a summary of common outcomes from μFE models, with proposed nomenclature and units. The most relevant primary outcomes include stiffness [kN/mm] and yield load, commonly referred to as the estimated failure load [kN]. A linear, elastic FE model intrinsically cannot directly measure failure load; however, non-linear approaches that are more appropriate for strength measurement are computationally demanding and therefore not often employed in high-resolution models [67, 75]. Instead, a failure criterion often used with linear FE models assumes bone yields when a specified volume of bone tissue (critical volume) exceeds a specified critical strain. This is often referred to as the "Pistoia criterion", and a typical set of yield parameters used assumes failure load can be estimated when the critical strain of 0.7% is exceeded for 2% for the bone tissue [76]; however, a complete table of commonly used yield parameters are provided in Table 4. Use of the Pistoia criterion for HR-pQCT-derived μFE models has led to strong correlations ($r^2 = 0.73$–0.95) with experimentally measured whole bone strength for the first-generation HR-pQCT [67, 77, 78], although some have suggested a 7.5% critical volume and 0.7% critical strain are more appropriate [77]. For the second-generation HR-pQCT, where scan volume and resolution differ, appropriate criterion needs to be adjusted [74]. A recent study by Arias-Moreno and colleagues determined that the appropriate failure criterion for the second-generation HR-pQCT should be a critical strain of 1.0% and critical volume of 5% under axial loading conditions [68]. Regardless of the specific parameters chosen, these variations of criteria provide highly comparable correlations with experimental bone strength and have been shown to be suitable predictors for failure load, but absolute values obtained using different yield parameters should not be directly compared. μFE-estimated failure load at the distal tibia scan site has also been shown to be well correlated to bone strength at the femoral neck and vertebra [79].

A common misconception is that μFE models predict failure load in a fall condition; however, boundary conditions in that scenario are prohibitively difficult to estimate with an enormous range of loading possibilities. Instead, standardized axial or uniaxial μFE tests of bone strength provide a reproducible approach that gives insight into the effect of bone microarchitecture on estimated bone strength. In addition to the failure load, there are several other μFE model outputs that provide additional insight into the biomechanical properties of bone, details are provided in Table 5.
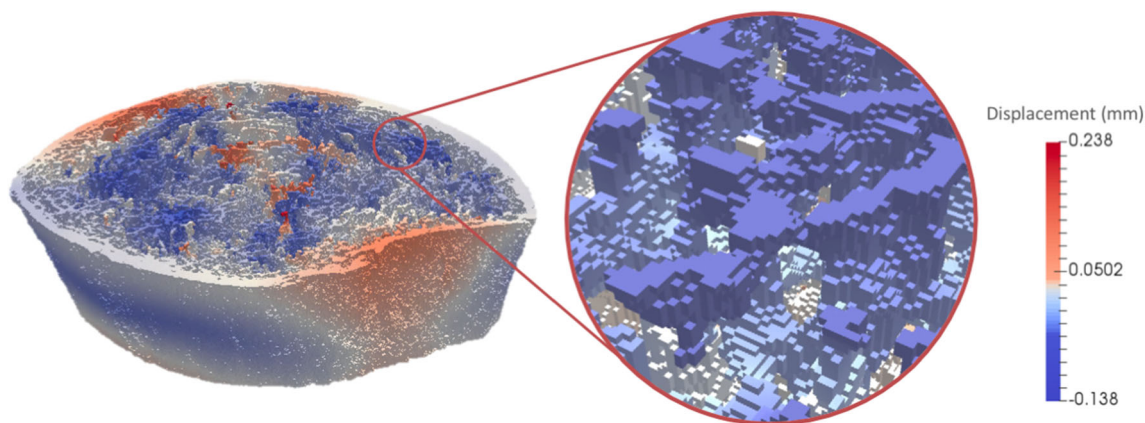
Fig. 4 Example of a segmented second-generation HR-pQCT tibia scan converted into an FE mesh using a voxel-by-voxel conversion approach. The model is composed of millions of hexahedral elements

In summary, for first-generation HR-pQCT, the choice of boundary conditions, elastic modulus, and yield criterion have varied among studies, but harmonization techniques are available to compare results using the different configurations summarized in Table 4 [74]. For the second-generation HR-pQCT, we recommend using an elastic modulus of 10,000 MPa with axial boundary conditions, and yield criterion of 1.0% critical strain and 5% critical volume. However, if this is not feasible, harmonization methods like those used for the first-generation HR-pQCT should be developed and used to compare results across studies [74]. As future systems become available, it will be necessary to determine the appropriate elastic modulus and yield criterion through back-calculation or direct validation for that particular system, ideally so that comparisons across HR-pQCT technologies are possible.

FE solvers

Due to the resolution of the images, μFE models tend to be very large, on the order of 10s of millions of degrees of freedom, and thus, the models pose a challenge for traditional commercial FE solvers. Fortunately, this problem has been overcome by the use of specialized solvers that are designed to leverage the fact that each element in the model (i.e., voxel) has the same hexahedral shape [80]. Scanco Medical provides built-in linear elastic FE software for the XtremeCT and XtremeCT II scanners, with libraries of pre-defined tests that may be applied. Specialized third-party FE solvers are also available that allow for faster computation time and flexibility, including commercial software (e.g., Numerics88 Solutions) as well as open-source versions (e.g., ParFE).

Table 4 Summary of elastic modulus, boundary conditions, and common yield criterion for first- and second-generation HR-pQCT. All models applied a 1% compressive strain in the axial direction and used a Poisson's ratio of 0.3. Unless specified, the proposed yield criterion and associated constitutive properties were compared with mechanical compressive loading tests; however, loading configurations relative to the scan region vary across studies [67–69, 74, 76, 77, 111]

Reference	Elastic modulus (MPa)	Boundary conditions	Yield criterion (critical strain, critical volume)
First-generation HR-pQCT			
Pistoia et al. Bone. 2002/Pistoia et al. J Clin. Dens. 2004[*]	10,000	Axial	0.7%, 2%
MacNeil et al. Bone 2008	6829	Uniaxial	0.7%, 2%
Mueller et al. Bone 2009	6829	Uniaxial	0.7%, 7.5%
Vilayphiou et al. Bone 2010[†]	Trabecular bone: 17,000 Cortical bone: 20,000	Axial	0.35%, 2%
Second-generation HR-pQCT			
Whittier et al. J Biomech 2018	8748	Uniaxial	0.7%, 2%
Arias-Moreno Osteoporosis Int 2019	10,000	Axial	1.0%, 5%

[*] Original validation studies were conducted using a 3D-pQCT scanner with 165 μm isotropic resolution; however, these parameter specifications have been frequently applied to first-generation HR-pQCT

[†] Yield criterion with associated tissue properties and boundary conditions were not explicitly validated in this study

Table 5 Definition, units, and measurement of methods of common micro-finite element analysis outcomes obtained from available HR-pQCT systems

Parameter	Abbreviation and standard units	Description
Primary model outputs		
Estimated failure load	FL (kN)	Estimate failure load is indirectly estimated from linear FE models using a yield criterion. When a specified volume of bone tissue (critical volume) exceeds a specified critical strain, the model is assumed to have yielded. This is often referred to as the Pistoia criterion.
Stiffness	Stiffness (kN/mm)	The total reaction force of the model divided by the applied displacement.
Additional model outputs		
Reaction force	RF (N)	The force required to induce the applied strain (typically 1%) in the model.
Compartment load distribution	$Load_{cort,dist}$ (%) $Load_{cort,prox}$ (%) $Load_{trab,dist}$ (%) $Load_{trab,prox}$ (%)	The ratio of the force carried by the trabecular and/or cortical compartments, at the distal and proximal ends of the model. It is sufficient to only report the load shared by one compartment, and the choice of reporting distal and/or proximal end is dependent on the research question.
Apparent modulus	E_a (kN/mm^2)	The average stress divided by the applied strain of the model. The average stress is the total reaction force divided by the average slice area. The applied strain is calculated as the applied displacement [mm] divided by the original height of the model (mm).
Tissue-level outputs[*]		
Average von Mises stress	$Stress_{VM}$ (MPa)	Scalar measure of the deviatoric stress accounting for the three principle axes. It can be used for yield criterion or as a heuristic measure of the magnitude of the stress at a given point.
Strain energy density	SED (J/mm^3)	The strain energy per unit volume of bone tissue. Strain energy is the increased energy associated with deformation in the FE model.

[*] These properties are scalar values defined for each element. Properties can be visualized on the model to inspect localized stress and strains, or expressed in terms of histograms. The average or median value across the model can be reported, and the histogram skewness or kurtosis can be used to provide insight into the strain distributions in the context of bone adaptation

Assumptions

It is important to be aware that µFE carries assumptions about tissue behavior. For instance, in µFE models, bone is assumed to be isotropic and behave purely linearly, both of which are only approximations of the true case. If applied to the atypical bone, this could possibly result in erroneous assumptions about bone strength in certain circumstances (e.g., osteogenesis imperfecta, fracture healing, or altered tissue-level properties) and care must be taken in designing studies and interpreting µFE results in these cases.

Image registration for longitudinal studies

A growing number of studies are producing longitudinal data to evaluate the effects of aging [10, 81] as well as pharmacologic [19, 82] or exercise interventions [25]. Small differences in participant positioning in follow-up

scans can result in variations of axial position and in the degree of tilt, illustrated in Fig. 5, and this reduces the ability to detect longitudinal change, particularly for parameters that vary considerably along the length of the bone (e.g., cortical geometry). Despite procedures to ensure that positioning is standardized as much as possible during each image acquisition, small variations in the scan region are inevitable. Consequently, reproducibility has been shown to be suboptimal with precision errors for trabecular and cortical parameters of up to 7.0% and 20.3% RMS-CV% respectively in the radius [83]. Registration techniques reduce positioning errors and are necessary in longitudinal studies to ensure the same region of the image is analyzed at each time point.

2D registration

A common 2D registration technique uses the total cross-sectional area of each slice to determine an optimal offset

between paired (baseline and follow-up) scans resulting in a common volume of interest with a subset of the original slices acquired [56]. This 2D technique is implemented in the Scanco software. It is capable of correcting for discrepancies in an axial direction, but cannot take into consideration the variation in tilt of the limb (Fig. 5). Notably, the 2D registration technique precludes evaluation of periosteal bone apposition and thus limits the interpretation of studies where a change in bone size is anticipated, such as growth, exercise, or perhaps aging over an extended observation.

3D registration

Methods using 3D rigid registration account for both positional (axial) and angular differences in images by determining the necessary 3D transform (translational and rotational) between two images. The method is based on optimally overlapping all image data within a volume of interest (e.g., within the periosteal contours) and so noise or structures outside the bone of interest do not impact registration. It is somewhat more complex to implement because it requires an optimization process, typically including a pre-alignment (e.g., based on the center of masses of the two images) followed by an optimizer-guided alignment based on a metric of best overlap (e.g., mutual information), ultimately resulting in a 3D transform matrix [84]. Strategies to maximize efficiency and minimize risk of errors include using downscaled images for initial alignment, and then increasing to full resolution to refine the alignment. Nevertheless, as with any automated process, it can result in errors and therefore it is imperative to visually assess the degree of overlap to ensure a reasonable solution has been achieved. The resulting 3D transform is used to identify a common region between multiple scans in a series, and the masks for that region are transformed, rather than the images themselves, to prevent image degradation associated with interpolation [84]. Currently, the 3D registration procedures are not part of the standard Scanco software.

While 3D registration provides excellent reproducibility for morphological parameters, it is unfortunately not as effective for μFE analysis. The application of boundary conditions to non-parallel surfaces resulting from common regions of interest from 3D registration in μFE models is not trivial, and currently, there is ongoing research in this area. To date, reproducibility of μFE outputs has not been found to be greater with 3D than 2D registration; therefore, use of 3D registration is not yet recommended for μFE [84]. Instead, the recommended approach is to apply μFE to 2D registered data, but only relative changes should be compared in this context and not absolute outcomes, as a shorter segment of bone will yield different results from a full-height image. If absolute outcomes are to be compared, unregistered data should be used for μFE analyses and comparisons.

Additional considerations for image registration

Typically, in longitudinal studies, the periosteal and endocortical surfaces are defined independently between baseline and follow-up scans. However, in some cases, it may be preferable to compare changes in a fixed region over time, such as for detecting trabecularization of the cortical region. This can be accomplished by taking the defined cortical and trabecular regions at baseline and applying these to the follow-up scans (in lieu of re-defining the regions independently) [85]. This method ensures the exact same region of bone is compared between baseline and follow-up. Consequently, this approach precludes detecting changes in cortical thickness, perimeter, or changes in total, cortical, or trabecular areas. When conducting 3D registration, it is important to specify if trabecular and cortical compartments were defined independently or if regions were defined at baseline and applied during registration on follow-up scans.

There are circumstances where the value of registration may be diminished. In long-term treatment and aging studies, there can be significant changes in bone geometry and microstructure. This can lead to inaccuracies when using both 2D and 3D registration. Consequently, shorter intervals may be required to allow sequential transformations to take place, with smaller incremental changes, to allow a more optimal

Fig. 5 Examples of axial (**a**) and angular (**b**) offsets in between scan regions captured at baseline (blue) and follow-up (red)
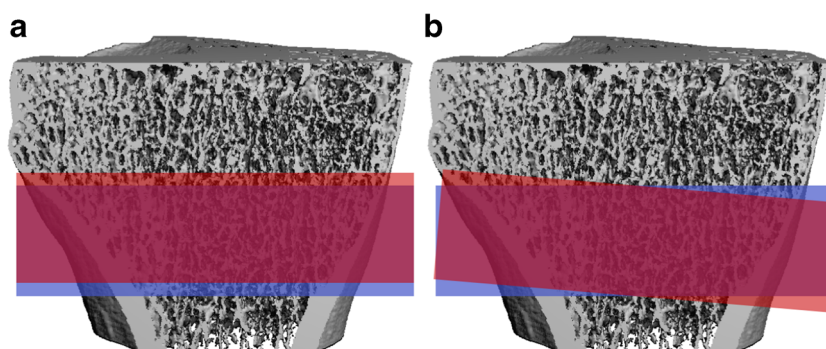
comparison of bone health between the start and end of the study. Furthermore, in children, bone growth leads to challenges because a fixed distance from the endplate will gradually become a more distal part of the bone and bone size is anticipated to change substantially [86]. Lastly, in the case of fracture healing, rapid remodeling occurs that changes overall bone geometry [71, 87] which poses challenges in terms of image registration and longitudinal comparison of bone morphology. It is imperative to visually inspect registered images to confirm that unexpected errors have not occurred during registration before the quantitative assessment is performed.

In general, follow-up scans should be registered to ensure the equivalent region is assessed, where 3D registration is the preferred method; however, if this approach is not feasible, 2D registration is an acceptable alternative. In both cases, a reasonable level of overlap must exist to include results from morphological or µFE analysis, so that the region is representative of the full scan length. An optimal minimum overlap between baseline and follow-up scans has not been validated, but we recommend a minimum volumetric overlap of 75%. There are circumstances where in a series of multiple follow-up scans there is one scan that is poorly positioned (i.e., less than 75% overlap). Rather than removing the entire series, that single scan can be removed so that the remainder of the subject's data can be used in the analysis. The choice of overlap cut-off should be specified in the study design and median or average overlap reported in the results.

Reporting results

Reporting density and morphometric data

The decision of which density and microarchitecture parameters to report depends on the research question. Nevertheless, with the goal of developing standardized procedures for using HR-pQCT in clinical studies, a minimum set of parameters should be reported to appropriately characterize the trabecular and cortical bone. As the research field shifts from the first-generation to the second-generation HR-pQCT, appropriate terminology is necessary, as certain morphological parameters, such as Tb.Th, have fundamentally different methods of measurement between scanner generations and thus cannot be directly compared.

Historically, with the introduction of direct 3D morphological measures, bone microarchitecture that was measured directly instead of derived was denoted with an asterisk (e.g., Tb.Sp*) [61]. However, this naming convention has not been used consistently in the literature. As direct measurement becomes more commonplace with regular use of the extended cortical analysis protocol and shift towards the second-generation HR-pQCT, we propose instead that direct measures be denoted without an asterisk (e.g., Tb.Sp), whereas derived measures be identified with the superscript "d" (e.g., Tb.Sp^d). Although the type of measurement method can often be inferred based on the scanner generation, it is more appropriate to use explicit nomenclature. Although inconsistencies exist in literature to date, this approach will help avoid confusion in future studies. For example, Ct.Th can be measured directly or derived using the first-generation HR-pQCT scanner, but if not explicitly stated it is not clear which approach was used. Tables 2 and 3 provide a summary of recommended terminology for common indices for future studies, and the minimum set of parameters to be reported are provided in bold.

Reporting µFE data

The choice of reported µFE outputs should be chosen with consideration of what biomechanical properties are most relevant to the research question. In many cases, µFE outputs are highly correlated, and it is not advised to report all available parameters without reasonable justification. Commonly reported parameters for standard HR-pQCT scans are summarized in Table 5. Primary outcomes are strength estimates (such as failure load) and stiffness; it is recommended at least one of these parameters is reported at a minimum; however, it is usually not necessary to report both due to high correlation (i.e., $r > 0.9$). Other insightful parameters include load distribution properties, specifically compartment load sharing at the distal and proximal ends of the scan region, or in certain cases stress/strain distributions within the model. As µFE outputs are highly dependent on model properties and loading conditions, it is important to provide sufficient details of the µFE analysis conducted (as summarized in Table 4) as well as the mesh generation method, and computational solver used. Additional information that is beneficial to report, especially for non-standard scan sites or techniques, is the model complexity (usually reported and the average number of elements in the models), the average computation time per model, and specifications of the computing system (i.e., hardware) used.

Precision error

An important factor in the clinical application of HR-pQCT is its ability to produce highly precise and accurate results. Precision error arises from a combination of technical and operational factors and is specific to the scanner, parameter, operator(s), and study design. As discussed throughout this article, important contributors to precision error are motion artifacts [49, 51], subject positioning and reference line placement [42], manual correction of periosteal and endocortical contours [58, 59, 88], and use of registration techniques [84]. Precision error is most often reported as the root-mean-squared coefficient of variance (RMS-CV%) of

repeated measurements in a group of individuals. Reported ranges of short-term precision for first- and second-generation HR-pQCT are summarized in Table 6 [27]. Although these ranges provide an idea of expected precision error, it is nevertheless dependent on the individual scanner and operators, and precision should be determined for each scanner and research center in a manner that reflects the study design. For cross-sectional study designs, precision should be measured without registration techniques applied. Longitudinal studies should report precision values with registration applied in a manner that reflects the technique that will be applied to the dataset. In addition, the precision measurements should be conducted on a cohort that reflects the demographics of the study (i.e., elderly versus younger subjects).

Reporting results from longitudinal studies

When reporting results for longitudinal studies, the method used for image registration should be reported, along with the average amount of overlap obtained between accepted baseline and follow-up scans, and the number of scans or subjects excluded from the analyses due to poor overlap. Depending on the study design, investigators may also consider reporting results in comparison with the least significant change (LSC), defined as the minimum change observed in an individual that can be considered statistically significant ($p < 0.05$), calculated by multiplying precision error by 2.77 [89]. A summary of ranges reported for LSC (primarily from the first-generation XtremeCT) is provided in Table 6; however, LSC should be estimated from the precision error of the specific scanner and registration methods used.

Considerations for multiple comparisons

Due to the large number of parameters that are produced using HR-pQCT and high correlation between some parameters,

studies are susceptible to the issue of multiple comparisons and falsely positive statistical tests, or type I error. For example, there are often at least 11 parameters that are presented in HR-pQCT studies (see Tables 2 and 3) and this number is multiplied by two when examining both the radius and tibia. If a p value threshold of 0.05 is used to denote statistical significance between groups, then it is expected that by chance at least one comparison may be significant, when in reality it is not. When reporting results, investigators must interpret their results with this in mind.

Although there are no specific recommendations for how to address this issue, one approach could be to formally control for the potential of false-positive statistical tests, with the selection of statistical test dependent on the study design and power. The most conservative approach would be a Bonferroni correction, an alternate option is the Benjamini-Hochberg correction, which is advantageous as it accounts for the false discovery rate with a limited impact on power. It also favors large studies and it is easy to implement [90, 91]. Another way to preserve power in small studies could be to use a hierarchical method, adjusting for the false discovery rate [92]. Though not commonly employed for HR-pQCT studies, this method has the theoretical advantage of relying on a priori hypotheses in the analysis of HR-pQCT data. For instance, a first step could be to test for differences in total density, then in trabecular and cortical density if the comparison of total density is significant. Thereafter, the various parameters of each compartment can be tested if there is a significant difference for the compartment [93].

Quality control and training

Routine steps should be taken to ensure that the HR-pQCT system is working properly, and operators should be trained appropriately. The system should undergo routine service and maintenance check by the manufacturer annually.

Table 6 Precision error ranges, reported as the RMS-CV%, for first-generation (XtremeCT) and second-generation (XtremeCT II) scanners. First-generation ranges are from the meta-analysis conducted by Mikolajewicz and colleagues [27], and second-generation ranges were obtained from short-term reproducibility studies conducted to date [33, 88, 112]

Parameter	XtremeCT		XtremeCT II	
	Short-term precision (%)	LSC (%)	Short-term precision (%)	LSC (%)[†]
Density measurements	0.8–2.0	2.0–5.6	0.4–2.4	1.1–6.6
Area measurements	2.3–4.0	6.2–11.0	0.4–3.3	1.1–9.1
Trabecular microarchitecture	4.1–4.9	11.3–13.6	0.8–2.7	2.2–7.5
Cortical thickness	1.6–3.6	4.4–9.9	1.1–2.9	3.0–8.0
Cortical porosity	6.2–12.5	17.1–34.5	11.0–13.7	30.5–37. 9
µFE outputs	2.0–3.5	5.4–9.6	0.9–1.3	2.5–3.6

[†] LSC values were calculated by multiplying reported short-term precision error by 2.77

Daily and weekly quality control

The user should follow the manufacturer's protocol for quality control to ensure the system is functioning properly. This typically includes daily and weekly scans of a quality control phantom to check performance prior to in vivo scanning and to monitor the stability of density and microarchitecture parameters. A drift over time in the phantom measurements signals decay in the X-ray emission, which has the potential to confound longitudinal studies if not addressed. Use of Shewhart charts to track scanner stability is recommended, and although no specific guidelines for when a scanner should be recalibrated have been developed, typical changes on the order of 1.5% from the mean phantom density are considered a threshold for when an intervention should take place. Daily quality control scans should also be inspected visually to identify common artifacts, such as ring artifacts, or distortions that would affect measurement outcomes. These should only be corrected by the manufacturer during routine maintenance, but it is prudent for the user to carefully monitor image quality control.

Operator training

Operator training is an essential aspect of obtaining high-quality data. Although there is no formal training course or certification for operators of the HR-pQCT device, it is recommended that new operators undergo thorough training from experienced operators in patient management and positioning, location of the reference line, and manual correction of contours generated by the automated and semi-automated protocols. Unfortunately, limited formal training is available despite the knowledge that scan precision and inter-operator variability can be reduced using a standard training platform [42]. In terms of reference line placement, it is recommended that new operators complete the online training developed by UCSF (http://webapps.radiology.ucsf.edu/refline/) [42]. Comparable training for contouring has yet to be developed, and so it is recommended new operators receive training from an experienced operator, and guidelines previously reported be followed to minimize error bias [57]. In the future, standardized training courses should be offered.

Other considerations

Multi-center studies

Measurement of multi-center precision and cross-calibration is important when pooling data from multiple research groups and scan sites, as inter-scanner differences are a key source of error. When compared with single-center precision, HR-pQCT parameters are less precise across different scanners,

which may be attributed to differences in quality control of scanners, calibration, and intrinsic manufacturer differences. Burghardt and colleagues reported LSC values for the first-generation HR-pQCT ranging from two to five times that of short-term single-center precision [94]. There is some evidence in that second-generation HR-pQCT scanners have notably improved inter-scanner precision, resulting in differences below LSC [95]. However, this may not apply broadly and cross-calibration procedures should still be employed for future studies using second-generation HR-pQCT. Although no standardized procedure exists for the estimation of multi-center precision, the use of a phantom that mimics geometry, microarchitecture, and composition of standard scan regions is recommended for cross-calibration [94]. This information collected can be employed to establish cross-calibration procedures to minimize inter-scanner errors; however, individual approaches vary and there is currently no standardized approach. Optimal methods for cross-calibration in multi-center studies have not yet been established and studies in this area are greatly needed. Of note, the issue of multi-center calibration is more important for cross-sectional studies; in longitudinal studies that have primary outcomes of individual change, the concern for inter-scanner variation is lessened.

Adjusting for different scanner generations

The introduction of the second-generation HR-pQCT poses a challenge of comparing research findings across different systems. Factors such as differences in resolution, scan region of interest, and measurement methods make it challenging to compare data from different generations, and this will be further confounded when future systems become available. Although it is possible for the second-generation HR-pQCT to be operated in a configuration mimicking the original system, this is not ideal because it defeats the purpose of having improved signal-to-noise and better quality images. Cross-calibration between scanner generations has demonstrated that some parameters from the first-generation can be converted to equivalent parameters for the second-generation; however, some parameters such as Tb.Th, which are highly dependent on resolution, should not be compared across systems [29, 33].

Beam hardening and scatter

Beam hardening and scatter effects that arise due to increased adipose (fat) tissue overlying the scan region, as might be expected in an obese population, can introduce measurable bias in HR-pQCT parameters [96]. Specifically, overlying adipose tissue can result in underestimation of density measurements and failure load, and altered trabecular microarchitecture, often leading to overestimation of bone microarchitecture impairment [96]. Similarly, high-density objects such as a clinical cast composed of plaster-of-Paris

or fiberglass can result in similar bias, due to beam hardening effects, and should be accounted for in a quantitative analysis if they are present in the scan [97, 98]. Future work is needed to determine the appropriate standardized procedures for overweight and obese individuals.

Bone tissue mineralization

Variations in bone tissue mineralization can influence morphological measurements obtained from HR-pQCT. Extraction of the bone structure uses a fixed threshold technique, and consequently, under-mineralized bone tissue that falls below the threshold may not be captured. In addition, μFE analysis usually assumes a uniform tissue modulus for all of the bone, and thus, variation in the degree of mineralization is not accounted for in bone strength estimates. Typical variability in tissue mineralization has little effect on morphological or μFE-derived outcomes [67, 99]. However, results must be interpreted carefully in situations that produce more extreme values of tissue mineralization, such as metabolic bone diseases (e.g., osteopetrosis) or pharmacologic treatments. In particular, induction of new bone formation by anabolic therapies may lead to a relatively undermineralized bone matrix, whereas potent anti-remodeling drugs lead to an increase in tissue mineralization.

Other high-resolution systems

The HR-pQCT systems discussed here focuses on available systems, manufactured by Scanco Medical AG. It is expected that HR-pQCT systems developed by other manufacturers will become available in the near future. In addition, existing imaging technologies are being adapted to study extremity bone microarchitecture as a substitute to HR-pQCT, namely cone-beam CT (CBCT) [100–103]. Current CBCT systems designed for extremity scanning offer larger scan lengths and shorter scanning times relative to HR-pQCT, with some systems allowing for scan acquisition in a weight-bearing configuration [103]. These benefits come with the trade-off of lower resolution, typically 127-μm nominal resolution reconstructed to a 75-μm voxel size [100]. Consequently, CBCT is susceptible to partial volume effects and can struggle to distinguish thinner trabecular structures that are visible with HR-pQCT [102]. As the application of CBCT for bone microarchitecture grows, and new HR-pQCT systems become available, the recommendations and guidelines outlined in this article should be considered.

Table 7 Summary of recommendations

Scan acquisition and analysis

- *The method of selecting scan site should be clearly indicated.* The relative offset outlined in this article and described in detail elsewhere [36] is recommended; however, a fixed offset may be used when comparing to historical datasets.

- *Image processing should use direct measurement methods following the extended cortical analysis.* Automatically generated contours should be checked and manually corrected for errors following guidelines outlines in detail elsewhere [57].

- *μFE analysis should use standardized constitutive properties and boundary conditions.* μFE specifications outlined in Table 4 are recommended for first-generation HR-pQCT and can be compared using harmonizing techniques. For second-generation HR-pQCT analysis, an elastic modulus of 10,000 MPa with axial boundary conditions and a yield criterion of 1.0% critical strain and 5% critical volume is recommended.

- *Longitudinal studies should employ 3D or 2D registration and exclude scans with less than 75% overlap.* μFE should not be applied to 3D-registered scans and instead 2D-registered or unregistered scans should be used.

Reporting results

- *Standardized nomenclature proposed here should be used for reporting results.* Nomenclature proposed in Tables 2, 3, and 5 should be used, and use of direct or indirect measurement techniques should be clearly indicated. The minimum parameters to describe trabecular bone morphology should include trabecular bone volume fraction, and trabecular number, thickness, and separation; for cortical bone morphology, cortical thickness, and cortical porosity should be reported.

- *Precision error should be measured and reported for each research center, specific to study protocol.* Cross-sectional studies should report precision with unregistered scans, and longitudinal studies should report precision with the registration technique used in the study design.

Quality control and training

- *Quality control should follow manufacturer maintenance protocol, including daily and weekly scanning of QC phantoms.* Scanner drift should be actively monitored, and the use of Shewhart charts to track scanner stability is recommended.

- *New operators should be trained by an experienced operator and available training tools used.* New operators should be trained in patient management and positioning, anatomical measurements, location of the reference line, and manual correction of contours generated by the automated and semi-automated protocols. Training should be supplemented with online reference line training developed by UCSF [42], and other online resources, as they become available.

- *Continuity across scanner generations (makes, models) should be assessed through cross-calibration.* It is important to understand relationships between parameters measured on different scanner generations [29, 33]. Typically, density-based parameters can be converted between scanner generations, but resolution-dependent parameters (e.g., Tb.Th) are problematic and should not be compared between generations.

- *Multi-center studies should report inter-scanner precision error*, and it is recommended that these are estimated using a calibration phantom that replicates geometry, densities, and microarchitecture of standard scan sites.

Pediatric studies

There is growing interest in the application of HR-pQCT in pediatrics for the study of normal skeletal acquisition [8], as well as the impact of disease [15] and physical activity [24] on skeletal acquisition. However, measurement of bone density and microarchitecture in children and adolescents poses unique challenges due to the complexities of long bone growth and presence of the growth plate near the scan region [86]. Non-linear bone growth and differences in maturation between sexes and ethnicities pose challenges in the appropriate selection of a standardized scan region. Several protocols have been proposed for the selection of the scan region to account for long bone growth [104], and although there is no consensus regarding the most appropriate scan site, there is an agreement that a relative offset should be used in children and adolescents. Further work is required to form a consensus on a standardized protocol for pediatric studies, including how to handle the transition from a pediatric to adult scanning protocol in longitudinal studies where participants are followed from childhood into adulthood.

Non-standard applications

HR-pQCT is specifically designed to measure the distal radius and distal tibia in adults, but its application to study bone microarchitecture at other sites has expanded in recent years. The introduction of XtremeCT II, which has a larger gantry and redesigned staging mechanism, permits knee and elbow joints to be imaged [105]. Furthermore, applications beyond the standard protocol have included the study of fracture healing at the distal radius [71], quantification of muscle morphometry [47], progression of inflammatory arthritis through quantification of joint space narrowing and development of erosions in finger and wrist joints [106, 107], and investigation of changes in bone microarchitecture at the knee due to injury or osteoarthritis [108]. These emerging applications are likely to become more prominent in HR-pQCT research and will require careful development of standardized protocols. A prominent example of this is the development of research focused on inflammatory arthritis, with as many as 20 research centers actively publishing in this area. Ongoing standardization of this novel application is overseen by the international consortium, SPECTRA (Study grouP for xtrEme-Computed Tomography in Rheumatoid Arthritis) [109, 110].

Summary of recommendations

Recommendations for best practices for the acquisition and analysis of HR-pQCT imaging techniques have been presented here, with nomenclature and recommendations on presenting and interpreting results. Many decisions on appropriate techniques and study design remain dependent on the research question. However, with the uptake in the clinical application of HR-pQCT, a certain degree of standardization is necessary to support the further advancement of the clinical application of HR-pQCT. The key recommendations for standard analysis of the distal radius and tibia HR-pQCT scans are summarized in Table 7. Implementation of these recommendations as "best practices" should facilitate the comparison of results across studies by minimizing technical variation in scan acquisition and analysis.

Compliance with ethical standards

Conflicts of interest Dr. Boyd is a co-founder and co-owner of Numerics88 Solutions Inc., creator of finite element package FAIM. Dr. Ghasem-Zadeh is one of the inventors of the StrAx algorithm and consults for Strax Corp. Dr. Burghardt is a consultant and served on an Advisory Board to Mereo BioPharma.

References

1. Boutroy S, Bouxsein ML, Munoz F, Delmas PD (2005) In vivo assessment of trabecular bone microarchitecture by high-resolution peripheral quantitative computed tomography. J Clin Endocrinol Metab 90:6508–6515
2. Jobke B, Burghardt AJ, Muche B, Hahn M, Semler J, Amling M, Majumdar S, Busse B (2011) Trabecular reorganization in consecutive iliac crest biopsies when switching from bisphosphonate to strontium ranelate treatment. PLoS One 6:e23638
3. Jobke B, Muche B, Burghardt AJ, Semler J, Link TM, Majumdar S (2011) Teriparatide in bisphosphonate-resistant osteoporosis: microarchitectural changes and clinical results after 6 and 18 months. Calcif Tissue Int 89:130–139
4. Burt LA, Bhatla JL, Hanley DA, Boyd SK (2017) Cortical porosity exhibits accelerated rate of change in peri- compared with post-menopausal women. Osteoporos Int 28:1423–1431
5. Burt LA, Liang Z, Sajobi TT, Hanley DA, Boyd SK (2016) Sex- and site-specific normative data curves for HR-pQCT. J Bone Miner Res 31:2041–2047
6. Burt LA, Macdonald HM, Hanley DA, Boyd SK (2014) Bone microarchitecture and strength of the radius and tibia in a reference population of young adults: an HR-pQCT study. Arch Osteoporos 9:183
7. Gabel L, Macdonald HM, McKay HA (2017) Sex differences and growth-related adaptations in bone microarchitecture, geometry, density, and strength from childhood to early adulthood: a mixed longitudinal HR-pQCT study. J Bone Miner Res 32:250–263
8. Gabel L, Macdonald HM, Nettlefold LA, McKay HA (2018) Sex-, ethnic-, and age-specific centile curves for pQCT- and HR-pQCT-derived measures of bone structure and strength in adolescents and young adults. J Bone Miner Res 33:987–1000
9. Hansen S, Shanbhogue V, Folkestad L, Nielsen MM, Brixen K (2014) Bone microarchitecture and estimated strength in 499 adult

Danish women and men: a cross-sectional, population-based high-resolution peripheral quantitative computed tomographic study on peak bone structure. Calcif Tissue Int 94:269–281

10. Macdonald HM, Nishiyama KK, Kang J, Hanley DA, Boyd SK (2011) Age-related patterns of trabecular and cortical bone loss differ between sexes and skeletal sites: a population-based HR-pQCT study. J Bone Miner Res 26:50–62

11. Popp KL, Hughes JM, Martinez-Betancourt A, Scott M, Turkington V, Caksa S, Guerriere KI, Ackerman KE, Xu C, Unnikrishnan G, Reifman J, Bouxsein ML (2017) Bone mass, microarchitecture and strength are influenced by race/ethnicity in young adult men and women. Bone 103:200–208

12. Vilayphiou N, Boutroy S, Sornay-Rendu E, Van Rietbergen B, Chapurlat R (2016) Age-related changes in bone strength from HR-pQCT derived microarchitectural parameters with an emphasis on the role of cortical porosity. Bone 83:233–240

13. Milovanovic P, Adamu U, Simon MJ, Rolvien T, Djuric M, Amling M, Busse B (2015) Age- and sex-specific bone structure patterns portend bone fragility in radii and tibiae in relation to osteodensitometry: a high-resolution peripheral quantitative computed tomography study in 385 individuals. J Gerontol A Biol Sci Med Sci 70:1269–1275

14. Bacchetta J, Boutroy S, Vilayphiou N, Juillard L, Guebre-Egziabher F, Rognant N, Sornay-Rendu E, Szulc P, Laville M, Delmas PD, Fouque D, Chapurlat R (2010) Early impairment of trabecular microarchitecture assessed with HR-pQCT in patients with stage II-IV chronic kidney disease. J Bone Miner Res 25:849–857

15. Braun C, Bacchetta J, Braillon P, Chapurlat R, Drai J, Reix P (2017) Children and adolescents with cystic fibrosis display moderate bone microarchitecture abnormalities: data from high-resolution peripheral quantitative computed tomography. Osteoporos Int 28:3179–3188

16. Nour MA, Burt LA, Perry RJ, Stephure DK, Hanley DA, Boyd SK (2016) Impact of growth hormone on adult bone quality in turner syndrome: a HR-pQCT study. Calcif Tissue Int 98:49–59

17. Samelson EJ, Demissie S, Cupples LA, Zhang X, Xu H, Liu CT, Boyd SK, McLean RR, Broe KE, Kiel DP, Bouxsein ML (2018) Diabetes and deficits in cortical bone density, microarchitecture, and bone size: Framingham HR-pQCT Study. J Bone Miner Res 33:54–62

18. Boyd SK, Burt LA, Sevick LK, Hanley DA (2015) The relationship between serum 25(OH)D and bone density and microarchitecture as measured by HR-pQCT. Osteoporos Int 26:2375–2380

19. Burghardt AJ, Kazakia GJ, Sode M, de Papp AE, Link TM, Majumdar S (2010) A longitudinal HR-pQCT study of alendronate treatment in postmenopausal women with low bone density: relations among density, cortical and trabecular microarchitecture, biomechanics, and bone turnover. J Bone Miner Res 25:2558–2571

20. Tsai JN, Nishiyama KK, Lin D, Yuan A, Lee H, Bouxsein ML, Leder BZ (2017) Effects of denosumab and teriparatide transitions on bone microarchitecture and estimated strength: the DATA-Switch HR-pQCT study. J Bone Miner Res 32:2001–2009

21. Langsetmo L, Shikany JM, Burghardt AJ et al (2018) High dairy protein intake is associated with greater bone strength parameters at the distal radius and tibia in older men: a cross-sectional study. Osteoporos Int 29:69–77

22. Burt LA, Billington EO, Rose MS, Raymond DA, Hanley DA, Boyd SK (2019) Effect of high-dose vitamin D supplementation on volumetric bone density and bone strength: a randomized clinical trial. JAMA 322:736–745

23. Burt LA, Schipilow JD, Boyd SK (2016) Competitive trampolining influences trabecular bone structure, bone size, and bone strength. J Sport Health Sci 5:469–475

24. Gabel L, Macdonald HM, Nettlefold L, McKay HA (2017) Physical activity, sedentary time, and bone strength from childhood to early adulthood: a mixed longitudinal HR-pQCT study. J Bone Miner Res 32:1525–1536

25. Hughes JM, Gaffney-Stomberg E, Guerriere KI, Taylor KM, Popp KL, Xu C, Unnikrishnan G, Staab JS, Matheny RW Jr, McClung JP, Reifman J, Bouxsein ML (2018) Changes in tibial bone microarchitecture in female recruits in response to 8weeks of U.S. Army Basic Combat Training. Bone 113:9–16

26. Kazakia GJ, Tjong W, Nirody JA, Burghardt AJ, Carballido-Gamio J, Patsch JM, Link T, Feeley BT, Ma CB (2014) The influence of disuse on bone microstructure and mechanics assessed by HR-pQCT. Bone 63:132–140

27. Mikolajewicz N, Bishop N, Burghardt AJ et al (2019) HR-pQCT measures of bone microarchitecture predict fracture: systematic review and meta-analysis. J Bone Miner Res

28. Stauber M, Müller R (2008) Micro-computed tomography: a method for the non-destructive evaluation of the three-dimensional structure of biological specimens. Methods Mol Biol 455:273–292

29. Agarwal S, Rosete F, Zhang C, McMahon DJ, Guo XE, Shane E, Nishiyama KK (2016) In vivo assessment of bone structure and estimated bone strength by first- and second-generation HR-pQCT. Osteoporos Int 27:2955–2966

30. Bandirali M, Lanza E, Messina C, Sconfienza LM, Brambilla R, Maurizio R, Marchelli D, Piodi LP, di Leo G, Ulivieri FM, Sardanelli F (2013) Dose absorption in lumbar and femoral dual energy X-ray absorptiometry examinations using three different scan modalities: an anthropomorphic phantom study. J Clin Densitom 16:279–282

31. Wylie JD, Jenkins PA, Beckmann JT, Peters CL, Aoki SK, Maak TG (2018) Computed tomography scans in patients with young adult hip pain carry a lifetime risk of malignancy. Arthroscopy 34(155–163):e153

32. Manske SL, Zhu Y, Sandino C, Boyd SK (2015) Human trabecular bone microarchitecture can be assessed independently of density with second generation HR-pQCT. Bone 79:213–221

33. Manske SL, Davison EM, Burt LA, Raymond DA, Boyd SK (2017) The estimation of second-generation HR-pQCT from first-generation HR-pQCT using in vivo cross-calibration. J Bone Miner Res 32:1514–1524

34. Wang Q, Wang XF, Iuliano-Burns S, Ghasem-Zadeh A, Zebaze R, Seeman E (2010) Rapid growth produces transient cortical weakness: a risk factor for metaphyseal fractures during puberty. J Bone Miner Res 25:1521–1526

35. Burrows M, Liu D, Moore S, McKay H (2010) Bone microstructure at the distal tibia provides a strength advantage to males in late puberty: an HR-pQCT study. J Bone Miner Res 25:1423–1432

36. Bonaretti S, Majumdar S, Lang TF, Khosla S, Burghardt AJ (2017) The comparability of HR-pQCT bone measurements is improved by scanning anatomically standardized regions. Osteoporos Int 28:2115–2128

37. Shanbhogue VV, Hansen S, Halekoh U, Brixen K (2015) Use of relative vs fixed offset distance to define region of interest at the distal radius and tibia in high-resolution peripheral quantitative computed tomography. J Clin Densitom 18:217–225

38. Boyd SK (2008) Site-specific variation of bone micro-architecture in the distal radius and tibia. J Clin Densitom 11:424–430

39. Hauspie RC, Vercauteren M, Susanne C (1997) Secular changes in growth and maturation: an update. Acta Paediatr Suppl 423:20–27

40. Ghasem-Zadeh A, Burghardt A, Wang XF, Iuliano S, Bonaretti S, Bui M, Zebaze R, Seeman E (2017) Quantifying sex, race, and age specific differences in bone microstructure requires measurement of anatomically equivalent regions. Bone 101:206–213

41. Sode M, Burghardt AJ, Pialat JB, Link TM, Majumdar S (2011) Quantitative characterization of subject motion in HR-pQCT images of the distal radius and tibia. Bone 48:1291–1297

42. Bonaretti S, Vilayphiou N, Chan CM, Yu A, Nishiyama K, Liu D, Boutroy S, Ghasem-Zadeh A, Boyd SK, Chapurlat R, McKay H, Shane E, Bouxsein ML, Black DM, Majumdar S, Orwoll ES, Lang TF, Khosla S, Burghardt AJ (2017) Operator variability in scan positioning is a major component of HR-pQCT precision error and is reduced by standardized training. Osteoporos Int 28: 245–257

43. Zebaze R, Ghasem-Zadeh A, Mbala A, Seeman E (2013) A new method of segmentation of compact-appearing, transitional and trabecular compartments and quantification of cortical porosity from high resolution peripheral quantitative computed tomographic images. Bone 54:8–20

44. Schafer AL, Burghardt AJ, Sellmeyer DE, Palermo L, Shoback DM, Majumdar S, Black DM (2013) Postmenopausal women treated with combination parathyroid hormone (1-84) and ibandronate demonstrate different microstructural changes at the radius vs. tibia: the PTH and Ibandronate Combination Study (PICS). Osteoporos Int 24:2591–2601

45. Cheung AM, Majumdar S, Brixen K, Chapurlat R, Fuerst T, Engelke K, Dardzinski B, Cabal A, Verbruggen N, Ather S, Rosenberg E, de Papp AE (2014) Effects of odanacatib on the radius and tibia of postmenopausal women: improvements in bone geometry, microarchitecture, and estimated bone strength. Journal of bone and mineral research : the official journal of the American Society for Bone and Mineral Research 29:1786–1794

46. Patsch JM, Burghardt AJ, Yap SP, Baum T, Schwartz AV, Joseph GB, Link TM (2013) Increased cortical porosity in type 2 diabetic postmenopausal women with fragility fractures. Journal of bone and mineral research : the official journal of the American Society for Bone and Mineral Research 28:313–324

47. Wong AK (2016) A comparison of peripheral imaging technologies for bone and muscle quantification: a technical review of image acquisition. J Musculoskelet Neuronal Interact 16:265–282

48. Stagi S, Cavalli L, Cavalli T, de Martino M, Brandi ML (2016) Peripheral quantitative computed tomography (pQCT) for the assessment of bone strength in most of bone affecting conditions in developmental age: a review. Ital J Pediatr 42:88

49. Engelke K, Stampa B, Timm W, Dardzinski B, de Papp AE, Genant HK, Fuerst T (2012) Short-term in vivo precision of BMD and parameters of trabecular architecture at the distal forearm and tibia. Osteoporos Int 23:2151–2158

50. Pauchard Y, Liphardt AM, Macdonald HM, Hanley DA, Boyd SK (2012) Quality control for bone quality parameters affected by subject motion in high-resolution peripheral quantitative computed tomography. Bone 50:1304–1310

51. Pialat JB, Burghardt AJ, Sode M, Link TM, Majumdar S (2012) Visual grading of motion induced image degradation in high resolution peripheral computed tomography: impact of image quality on measures of bone density and micro-architecture. Bone 50: 111–118

52. Laib A, Hauselmann HJ, Ruegsegger P (1998) In vivo high resolution 3D-QCT of the human forearm. Technol Health Care 6: 329–337

53. Davis KA, Burghardt AJ, Link TM, Majumdar S (2007) The effects of geometric and threshold definitions on cortical bone metrics assessed by in vivo high-resolution peripheral quantitative computed tomography. Calcif Tissue Int 81:364–371

54. Nishiyama KK, Macdonald HM, Buie HR, Hanley DA, Boyd SK (2010) Postmenopausal women with osteopenia have higher cortical porosity and thinner cortices at the distal radius and tibia than women with normal aBMD: an in vivo HR-pQCT study. Journal of bone and mineral research : the official journal of the American Society for Bone and Mineral Research 25:882–890

55. Buie HR, Campbell GM, Klinck RJ, MacNeil JA, Boyd SK (2007) Automatic segmentation of cortical and trabecular compartments based on a dual threshold technique for in vivo micro-CT bone analysis. Bone 41:505–515

56. Burghardt AJ, Buie HR, Laib A, Majumdar S, Boyd SK (2010) Reproducibility of direct quantitative measures of cortical bone microarchitecture of the distal radius and tibia by HR-pQCT. Bone 47:519–528

57. Whittier DE, Mudryk AN, Vandergaag ID, Burt LA, Boyd SK (2019) Optimizing HR-pQCT workflow: a comparison of bias and precision error for quantitative bone analysis. Osteoporos Int

58. Kawalilak CE, Johnston JD, Cooper DM, Olszynski WP, Kontulainen SA (2016) Role of endocortical contouring methods on precision of HR-pQCT-derived cortical micro-architecture in postmenopausal women and young adults. Osteoporos Int 27: 789–796

59. de Waard EAC, Sarodnik C, Pennings A, de Jong JJA, Savelberg HHCM, van Geel TA, van der Kallen CJ, Stehouwer CDA, Schram MT, Schaper N, Dagnelie PC, Geusens PPMM, Koster A, van Rietbergen B, van den Bergh JPW (2018) Reliability of HR-pQCT derived cortical bone structural parameters when using uncorrected instead of corrected automatically generated endocortical contours in a cross-sectional study: the Maastricht Study. Calcif Tissue Int 103:252–265

60. Hildebrand T, Rüegsegger P (1997) Quantification of bone microarchitecture with the structure model index. Comput Methods Biomech Biomed Engin 1:15–23

61. Hildebrand T, Laib A, Müller R, Dequeker J, Rüegsegger P (1999) Direct three-dimensional morphometric analysis of human cancellous bone: microstructural data from spine, femur, iliac crest, and calcaneus. J Bone Miner Res 14:1167–1174

62. Odgaard A, Gundersen HJ (1993) Quantification of connectivity in cancellous bone, with special emphasis on 3-D reconstructions. Bone 14:173–182

63. Whitehouse WJ (1974) The quantitative morphology of anisotropic trabecular bone. J Microsc 101:153–168

64. Liu XS, Sajda P, Saha PK, Wehrli FW, Bevill G, Keaveny TM, Guo XE (2008) Complete volumetric decomposition of individual trabecular plates and rods and its morphological correlations with anisotropic elastic moduli in human trabecular bone. J Bone Miner Res 23:223–235

65. Jorgenson BL, Buie HR, McErlain DD, Sandino C, Boyd SK (2015) A comparison of methods for in vivo assessment of cortical porosity in the human appendicular skeleton. Bone 73:167–175

66. van Rietbergen B, Ito K (2015) A survey of micro-finite element analysis for clinical assessment of bone strength: the first decade. J Biomech 48:832–841

67. MacNeil JA, Boyd SK (2008) Bone strength at the distal radius can be estimated from high-resolution peripheral quantitative computed tomography and the finite element method. Bone 42: 1203–1213

68. Arias-Moreno AJ, Hosseini HS, Bevers M, Ito K, Zysset P, van Rietbergen B (2019) Validation of distal radius failure load predictions by homogenized- and micro-finite element analyses based on second-generation high-resolution peripheral quantitative CT images. Osteoporos Int 30:1433–1443

69. Pistoia W, van Rietbergen B, Lochmuller EM, Lill CA, Eckstein F, Rüegsegger P (2002) Estimation of distal radius failure load with micro-finite element analysis models based on three-dimensional peripheral quantitative computed tomography images. Bone 30:842–848

70. Christen D, Zwahlen A, Müller R (2014) Reproducibility for linear and nonlinear micro-finite element simulations with density derived material properties of the human radius. J Mech Behav Biomed Mater 29:500–507

71. de Jong JJ, Willems PC, Arts JJ, Bours SG, Brink PR, van Geel TA, Poeze M, Geusens PP, van Rietbergen B, van den Bergh JP (2014) Assessment of the healing process in distal radius fractures by high resolution peripheral quantitative computed tomography. Bone 64:65–74

72. Engelke K, van Rietbergen B, Zysset P (2016) FEA to measure bone strength: a review. Clinic Rev Bone Miner Metab 14:26–37

73. Müller R, Rüegsegger P (1995) Three-dimensional finite element modelling of non-invasively assessed trabecular bone structures. Med Eng Phys 17:126–133

74. Whittier DE, Manske SL, Kiel DP, Bouxsein M, Boyd SK (2018) Harmonizing finite element modelling for non-invasive strength estimation by high-resolution peripheral quantitative computed tomography. J Biomech 80:63–71

75. Christen D, Melton LJ 3rd, Zwahlen A, Amin S, Khosla S, Muller R (2013) Improved fracture risk assessment based on nonlinear micro-finite element simulations from HRpQCT images at the distal radius. Journal of bone and mineral research : the official journal of the American Society for Bone and Mineral Research 28:2601–2608

76. Pistoia W, van Rietbergen B, Lochmuller EM, Lill CA, Eckstein F, Rüegsegger P (2004) Image-based micro-finite-element modeling for improved distal radius strength diagnosis: moving from bench to bedside. J Clin Densitom 7:153–160

77. Mueller TL, Christen D, Sandercott S, Boyd SK, van Rietbergen B, Eckstein F, Lochmuller EM, Muller R, van Lenthe GH (2011) Computational finite element bone mechanics accurately predicts mechanical competence in the human radius of an elderly population. Bone 48:1232–1238

78. Varga P, Pahr DH, Baumbach S, Zysset PK (2010) HR-pQCT based FE analysis of the most distal radius section provides an improved prediction of Colles' fracture load in vitro. Bone 47: 982–988

79. Kroker A, Plett R, Nishiyama KK, McErlain DD, Sandino C, Boyd SK (2017) Distal skeletal tibia assessed by HR-pQCT is highly correlated with femoral and lumbar vertebra failure loads. J Biomech 59:43–49

80. van Rietbergen B, Weinans H, Huiskes R, Odgaard A (1995) A new method to determine trabecular bone elastic properties and loading using micromechanical finite-element models. J Biomech 28:69–81

81. Chen H, Zhou X, Fujita H, Onozuka M, Kubo KY (2013) Age-related changes in trabecular and cortical bone microstructure. Int J Endocrinol 2013:213234

82. Seeman E, Delmas PD, Hanley DA, Sellmeyer D, Cheung AM, Shane E, Kearns A, Thomas T, Boyd SK, Boutroy S, Bogado C, Majumdar S, Fan M, Libanati C, Zanchetta J (2010) Microarchitectural deterioration of cortical and trabecular bone: differing effects of denosumab and alendronate. Journal of bone and mineral research : the official journal of the American Society for Bone and Mineral Research 25:1886–1894

83. Paggiosi MA, Eastell R, Walsh JS (2014) Precision of high-resolution peripheral quantitative computed tomography measurement variables: influence of gender, examination site, and age. Calcif Tissue Int 94:191–201

84. Ellouz R, Chapurlat R, van Rietbergen B, Christen P, Pialat JB, Boutroy S (2014) Challenges in longitudinal measurements with HR-pQCT: evaluation of a 3D registration method to improve bone microarchitecture and strength measurement reproducibility. Bone 63:147–157

85. Nishiyama KK, Pauchard Y, Nikkel LE, Iyer S, Zhang C, McMahon DJ, Cohen D, Boyd SK, Shane E, Nickolas TL (2015) Longitudinal HR-pQCT and image registration detects endocortical bone loss in kidney transplantation patients. J Bone Miner Res 30:554–561

86. Adams JE, Engelke K, Zemel BS, Ward KA, International Society of Clinical D (2014) Quantitative computer tomography in children and adolescents: the 2013 ISCD Pediatric Official Positions. J Clin Densitom 17:258–274

87. de Jong JJA, Christen P, Plett RM, Chapurlat R, Geusens PP, van den Bergh JPW, Müller R, van Rietbergen B (2017) Feasibility of rigid 3D image registration of high-resolution peripheral quantitative computed tomography images of healing distal radius fractures. PLoS One 12:e0179413

88. Chiba K, Okazaki N, Kurogi A, Isobe Y, Yonekura A, Tomita M, Osaki M (2018) Precision of second-generation high-resolution peripheral quantitative computed tomography: intra- and intertester reproducibilities and factors involved in the reproducibility of cortical porosity. J Clin Densitom 21:295–302

89. Shepherd JA, Lu Y (2007) A generalized least significant change for individuals measured on different DXA systems. J Clin Densitom 10:249–258

90. Benjamini Y, Hochberg Y (1995) Controlling the false discovery rate: a practical and powerful approach to multiple testing. J R Stat Soc Series B Stat Methodol 57:289–300

91. Boutroy S, Khosla S, Sornay-Rendu E, Zanchetta MB, McMahon DJ, Zhang CA, Chapurlat RD, Zanchetta J, Stein EM, Bogado C, Majumdar S, Burghardt AJ, Shane E (2016) Microarchitecture and peripheral BMD are impaired in postmenopausal white women with fracture independently of total hip T-score: an international multicenter study. J Bone Miner Res 31:1158–1166

92. Yekutieli D (2008) Hierarchical flse discovery rate-controlling methodology. J Am Stat Assoc 103:309–316

93. Gensburger D, Boutroy S, Chapurlat R, Nove-Josserand R, Roche S, Rabilloud M, Durieu I (2016) Reduced bone volumetric density and weak correlation between infection and bone markers in cystic fibrosis adult patients. Osteoporos Int 27:2803–2813

94. Burghardt AJ, Pialat JB, Kazakia GJ, Boutroy S, Engelke K, Patsch JM, Valentinitsch A, Liu D, Szabo E, Bogado CE, Zanchetta MB, McKay HA, Shane E, Boyd SK, Bouxsein ML, Chapurlat R, Khosla S, Majumdar S (2013) Multicenter precision of cortical and trabecular bone quality measures assessed by high-resolution peripheral quantitative computed tomography. J Bone Miner Res 28:524–536

95. Cauley JA, Burghardt AJ, Harrison SL, Cawthon PM, Schwartz AV, Connor EB, Ensrud KE, Langsetmo L, Majumdar S, Orwoll E, for the Osteoporotic Fractures in Men (MrOS) Research Group (2018) Accelerated bone loss in older men: effects on bone microarchitecture and strength. J Bone Miner Res 33:1859–1869

96. Caksa S, Yuan A, Rudolph SE, Yu EW, Popp KL, Bouxsein ML (2019) Influence of soft tissue on bone density and microarchitecture measurements by high-resolution peripheral quantitative computed tomography. Bone 124:47–52

97. de Jong JJ, Arts JJ, Meyer U, Willems PC, Geusens PP, van den Bergh JP, van Rietbergen B (2016) Effect of a cast on short-term reproducibility and bone parameters obtained from HR-pQCT measurements at the distal end of the radius. J Bone Joint Surg Am 98:356–362

98. Whittier DE, Manske SL, Boyd SK, Schneider PS (2018) The correction of systematic error due to plaster and fiberglass casts on HR-pQCT bone parameters measured in vivo at the distal radius. J Clin Densitom

99. MacNeil JA, Boyd SK (2007) Accuracy of high-resolution peripheral quantitative computed tomography for measurement of bone quality. Med Eng Phys 29:1096–1105

100. de Charry C, Boutroy S, Ellouz R, Duboeuf F, Chapurlat R, Follet H, Pialat JB (2016) Clinical cone beam computed tomography compared to high-resolution peripheral computed tomography in the assessment of distal radius bone. Osteoporos Int 27:3073–3082

101. Klintstrom E, Smedby O, Moreno R, Brismar TB (2014) Trabecular bone structure parameters from 3D image processing of clinical multi-slice and cone-beam computed tomography data. Skelet Radiol 43:197–204

102. Mys K, Varga P, Gueorguiev B, Hemmatian H, Stockmans F, van Lenthe GH (2019) Correlation between cone-beam computed tomography and high-resolution peripheral computed tomography for assessment of wrist bone microstructure. J Bone Miner Res 34: 867–874

103. Brehler M, Cao Q, Moseley KF, Osgood G, Morris C, Demehri S, Yorkston J, Siewerdsen JH, Zbijewski W (2018) Robust quantitative assessment of trabecular microarchitecture in extremity cone-beam CT using optimized segmentation algorithms. Proc SPIE Int Soc Opt Eng 10578:

104. Kawalilak CE, Bunyamin AT, Bjorkman KM, Johnston JD, Kontulainen SA (2017) Precision of bone density and micro-architectural properties at the distal radius and tibia in children: an HR-pQCT study. Osteoporos Int 28:3189–3197

105. Kroker A, Besler BA, Bhatla JL, Shtil M, Salat P, Mohtadi N, Walker RE, Manske SL, Boyd SK (2019) Longitudinal effects of acute anterior cruciate ligament tears on peri-articular bone in human knees within the first year of injury. J Orthop Res 37:2325–2336

106. Burghardt AJ, Lee CH, Kuo D, Majumdar S, Imboden JB, Link TM, Li X (2013) Quantitative in vivo HR-pQCT imaging of 3D wrist and metacarpophalangeal joint space width in rheumatoid arthritis. Ann Biomed Eng 41:2553–2564

107. Nagaraj S, Finzel S, Stok KS, Barnabe C, Collaboration S (2016) High-resolution peripheral quantitative computed tomography imaging in the assessment of periarticular bone of metacarpophalangeal and wrist joints. J Rheumatol 43:1921–1934

108. Kroker A, Zhu Y, Manske SL, Barber R, Mohtadi N, Boyd SK (2017) Quantitative in vivo assessment of bone microarchitecture in the human knee using HR-pQCT. Bone 97:43–48

109. Manske SL, Brunet SC, Finzel S, Stok KS, Conaghan PG, Boyd SK, Barnabe C (2019) The SPECTRA collaboration OMERACT working group: construct validity of joint space outcomes with high-resolution peripheral quantitative computed tomography. J Rheumatol 46:1369–1373

110. Stok KS, Finzel S, Burghardt AJ, Conaghan PG, Barnabe C, Collaboration S (2017) The SPECTRA collaboration OMERACT special interest group: current research and future directions. J Rheumatol 44:1911–1915

111. Vilayphiou N, Boutroy S, Sornay-Rendu E, Van Rietbergen B, Munoz F, Delmas PD, Chapurlat R (2010) Finite element analysis performed on radius and tibia HR-pQCT images and fragility fractures at all sites in postmenopausal women. Bone 46:1030–1037

112. Hosseini HS, Dunki A, Fabech J, Stauber M, Vilayphiou N, Pahr D, Pretterklieber M, Wandel J, Rietbergen BV, Zysset PK (2017) Fast estimation of Colles' fracture load of the distal section of the radius by homogenized finite element analysis based on HR-pQCT. Bone 97:65–75